Wear tests of hydrodynamic journal bearings lubricated with magnetorheological fluid

Wodtke, Michał; Litwin, Wojciech; van der Meer, Gerben; van Ostayen, Ron

DOI
10.1016/j.wear.2025.206404

Publication date
2026

Document Version
Final published version

Published in
Wear

Wear 584–585 (2026) 206404

Contents lists available at ScienceDirect

Wear

journal homepage: www.elsevier.com/locate/wear

Wear tests of hydrodynamic journal bearings lubricated with magnetorheological fluid

Michał Wodtke [a,b,*], Wojciech Litwin [a,b], Gerben van der Meer [c], Ron van Ostayen [c]

[a] EkoTech Center, Gdansk University of Technology, ul. Narutowicza 11/12, 80-233, Gdańsk, Poland
[b] Faculty of Mechanical Engineering and Ship Technology, Gdansk University of Technology, ul. Narutowicza 11/12, 80-233, Gdańsk, Poland
[c] Department of Precision and Microsystems Engineering, Delft University of Technology, Mekelweg 2, Delft, 2628 CD, the Netherlands

ARTICLE INFO

Keywords:
Wear
MR lubrication
Journal bearing
Wear mechanism

ABSTRACT

This research aimed to study the wear amount and mechanism of a hydrodynamic journal bearing lubricated with magnetorheological (MR) fluid. The effects of bearing load, hard particle content in the MR fluid, magnetic field activation, and bearing sleeve material were experimentally investigated. Results revealed that the standard bronze sleeve experienced extreme wear with MR lubrication, two orders of magnitude higher than for oil lubrication, while the friction coefficient was almost 6 times higher, probably due to severe third-body abrasion. The least amount of wear among all tested materials was observed with a more flexible polymer sleeve, which showed ~3.5 times more wear than the oil-lubricated bearing and a smaller increase in friction coefficient, around 2.6 times, as well as the formation of a possibly protective layer of crushed particles in the converging region of the film. The results suggest that polymers, and possibly also softer materials such as rubber, are a promising alternative for bearings lubricated with MR fluids under low-speed and high-load conditions.

1. Introduction

Magnetorheological (MR) fluids fall under the category of smart materials. They comprise a homogeneous suspension, consisting of dispersed magnetic medium (particles) in a non-magnetic carrier (e.g., water or mineral oil) and additives. What makes MR fluids unique is that their rheological properties can be actively and rapidly changed by activating a magnetic field (adjusting magnetic flux density). The magnetic field causes the formation of magnetic particle chain structures in the fluid which significantly increase its viscosity and can cause a transition from fluid-like to solid-like properties [1,2].

Due to strong development and research efforts, MR fluids found applications in many different mechanical devices, e.g., viscous couplings and clutches [3,4], dampers [5,6], or brakes [7,8]. One mechanical component that can exploit the benefits of MR fluid capabilities is the fluid-film bearing. Depending on the application, they can operate with the principle of a hydrodynamic wedge, or with the squeeze effect or hydrostatic effect, using common hydraulic oils as a lubricant to separate mating surfaces. This is one of their biggest advantages, since the fluid completely separates the sliding surfaces of the components and friction takes place inside the lubricant instead of between the sliding surfaces in the form of dry or mixed friction. Here it is important to note that fluid friction is the desirable type of friction due to low losses and lack of wear. The application of MR fluids as a lubricant in fluid-film bearings is one of the possible solutions for smart (intelligent) bearings [9–11]. The operating characteristics of smart bearings can be actively controlled or adjusted depending on the forces acting on the system, or the sliding velocity in the system. In the case of a MR bearing, changing the lubricant viscosity during operation by activating and adjusting the magnetic field brings a very attractive possibility to eliminate one of the biggest limitations of hydrodynamic bearings application, namely the very limited load-carrying capability at low-speed operation. By locally activating a magnetic field, it is possible to increase locally the viscosity in the lubricating film, thereby increasing the minimum film thickness. This to ensure more favourable conditions for the safety of bearing operation at high loads and low shaft speeds.

Experimental investigations of MR journal bearing properties for steady-state operation have generally confirmed those findings [12,13]. However, they revealed one limitation concerning journal speed; for high-speed values and thus for high values of MR fluid shear rates, the MR effect is significantly reduced (due to the shear-thinning effect) compared with the viscous effect [12,14]. In Ref. [15] the possibility of eliminating this disadvantage by using a special MR bearing design with a floating ring for enhanced stiffness and damping of the bearing system

* Corresponding author. EkoTech Center, Gdansk University of Technology, ul. Narutowicza 11/12, 80-233, Gdańsk, Poland.
E-mail address: michal.wodtke@pg.edu.pl (M. Wodtke).

https://doi.org/10.1016/j.wear.2025.206404
Received 5 February 2025; Received in revised form 22 October 2025; Accepted 24 October 2025
Available online 25 October 2025

was investigated. The experimental results showed that this bearing type remained controllable even when rotating at 1200 rpm. The MR effect was investigated in a thrust bearing configuration in steady-state mode to validate the theoretical model and predict the axial force as a result of the magnetic field [16]. The application of MR fluid was also experimentally investigated in the hydrostatic mode of lubrication. In Ref. [17], using an electromagnet, the magnetic field was applied locally at the outer edges of the hydrostatic bearing. This caused an increase in resistance in the MR fluid flow at the fluid film outlet zone, mimicking the behaviour of geometric textures, which resulted in a pressure profile shape in the MR fluid film similar to the profile in a geometrically textured hydrostatic bearing.

The authors of this paper also conducted experimental research on journal bearings lubricated with MR fluid on two separate test stands with differing shaft diameters (50 and 100 mm). Their results demonstrated that MR-lubricated hydrodynamic bearings can potentially solve problems of oil-lubricated bearings at high loads and low shaft speeds by ensuring locally tuned MR fluid viscosity [18]. It was also shown that applying a local magnetic field near the minimum film thickness can reduce losses to even lower values than those of the reference oil-lubricated bearing, while retaining a (small) increase in minimum film thickness [19]. However, after both investigations, clear signs of abrasive wear were noticed on the sliding surfaces of the MR-fluid lubricated bearing components. MR fluids are made of base oil and ferromagnetic, hard particles, which can influence bearing wear resistance, especially in mixed lubrication mode. This can be a huge disadvantage for MR bearings operating under low speed and high load, or for MR bearings experiencing frequent start/stop cycles. In other studies, wear problems for other sliding pairs utilising MR fluids, e.g. for O-ring sealings [20] have been investigated.

The effect of hard particles on lubrication performance has been investigated in the literature, as summarised in the works of Khonsari and Booser [21], and Nikas [22]. Their results showed that the particles dispersed in the lubricant worsen hydrodynamic performance by increasing friction losses, temperature, and wear on the sliding surface, which justifies the significance of proper filtration for the operation of lubricated surfaces [23]. The specific impact of iron particles dispersed in the lubricant (usually mineral oil) has been investigated experimentally as well [24–26]. The lubricant for such a case, in terms of the composition, was similar to MR fluid; however, it differed significantly in the iron particle content and size. Iron particle contamination in the reported tests varied from a handful of particles of large size (5–30 particles with sizes up to 1.4 mm, [24]) to 40–50 μm particles with a 0.05 % concentration by weight [25,26]. In contrast, the concentration of iron particles for MR fluid can reach 70 % by weight with an average particle size of only a couple of microns.

The wear mechanism of MR-fluid lubricated contacts has been studied extensively [27–33]; however, they did so only experimentally on the sample level using different contact configurations on tribometers. Their results provided many valuable findings, such as that measured wear and coefficient of friction for MR fluid-lubricated contacts were higher than for hydraulic oil [27] or that an increase in particle content in the MR fluid increased friction losses [28]. On the other hand, some contradictory conclusions concerning the effect of the magnetic field activation on tribological properties of MR-fluid lubricated sliding contacts were formulated in Refs. [29,30]. In Ref. [29], using a pin-on-disc tribometer, the MR fluid under a magnetic field shows better friction and wear properties compared to the absence of a magnetic field, while in the results of [30], utilising a four-ball tribological tester, the opposite trend was noticed. Most likely, these differences were due to the different geometry of the tested sliding pairs. Moreover, the effect of mating surface material [29] and material of the particles [31] on tribological performance was also studied, as well as comparative investigations with the tribological properties of other smart fluids, e.g. ferrofluids [32]. Finally, different types of solid lubricants added to silicone-based MR-fluid (e.g. PTFE, boron nitride, MoS_2 or graphite) were also investigated for the tribological performance using a four-ball geometry tribometer [33]. The results show that when MoS_2 was added to the MR fluid, the highest reduction in frictional force was obtained, while the addition of PTFE resulted in the least wear of the test samples. Several investigations also noticed that due to operation in mixed friction under tribological tests, not only were tested samples worn, but iron particles dispersed in MR fluid deformed and changed their initial shapes [27–29,34]. Wear of the MR fluid can also be an additional limitation for the long-term operation of the MR-bearing system operating under mixed friction mode.

The literature lacks wear test investigations under MR-fluid lubrication carried out on the component of interest in this paper, namely using hydrodynamic bearings. According to the authors' previous experimental results, this is one of the biggest challenges limiting the possibility of applying MR-lubricated bearings in low-speed conditions. This paper intents to fill that knowledge gap and reports the results of comprehensive tribological research on hydrodynamic bearings lubricated with MR fluid.

2. Goal of the research

This research aims to study the wear properties (wear mechanism and wear amount) of the components of a hydrodynamic bearing under varied bearing loads and operated with different MR lubricants, both with and without an activated magnetic field. Moreover, it aims to identify bearing sleeve materials capable of reducing the wear amount under MR lubrication to a level comparable to that of oil-lubricated bearings. For this comprehensive research project, an experimental study was conducted on a bearing system lubricated with standard and customised MR fluid. The research program involved long-time start/stop tests to assess the wear of the shafts and sleeves of the bearings. The wear assessment was based on the sliding surface geometry measurements before and after the tests. The sliding surfaces of the bearing sleeves and shaft journals were also examined using a scanning electron microscope (SEM) with integrated energy dispersive X-ray spectroscopy (EDS) to investigate the wear mechanisms and to check for possible material transfer between the two mating surfaces, and between the mating surfaces and the particles. SEM was also used to investigate the size and shape of the particles dispersed in the MR-fluid before and after the wear tests.

3. Methodology

3.1. Lubricant properties

The wear tests were carried out using three different lubricants, one mineral oil that was used as a reference, and two hydrocarbon-based MR fluids with different particle concentrations. For the reference measurements a standard maritime lubricating oil, Castrol MHP 153 (SAE 30), was used. The MR measurements were carried out with the standard MR fluid MRHCCS4-A with 70 % particle concentration by weight [35], as well as a variant of the same fluid with 20 % particle concentration by weight, which was designed at request by the same manufacturer. From now on these MR fluids will be referred to as 'MR 70 %' and 'MR 20 %' respectively.

The particle size distributions for both MR fluids were measured as well, see section 3.4 for the methodology and section 4.6 for the results. Do note that a different batch of smaller particles was used to create the MR 20 % fluid, and that the manufacturer indicated qualitatively that these particles were of a higher hardness than the particles used in the MR 70 % fluid. Fig. 1 shows several viscosity plots for these three lubricants. Fig. 1 a) shows viscosity as a function of temperature, for the MR fluids curves both with and without a magnetic field present are shown (Fig. 1). Furthermore, since the MR fluids are strongly shear-thinning, Fig. 1 b) shows the viscosity of all lubricants as a function of shear rate. Finally, Fig. 1 c) shows the change in viscosity when uniform

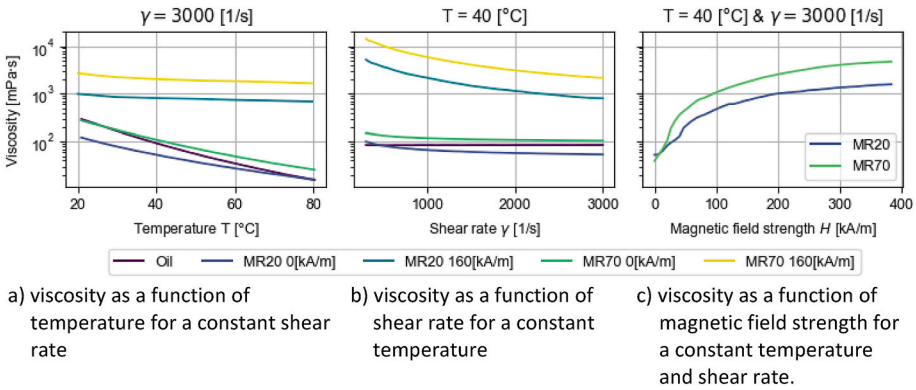

Fig. 1. Viscosity measurements for the three lubricants used in this paper.

magnetic fields of different strengths are applied to the two MR fluids. All viscosity measurements were performed with an Anton Paar MRC 302 rheometer with a cone on plate geometry.

3.2. Wear test setup

The custom-designed and built test rig for the wear test of the journal bearings with a 30 mm diameter shaft is presented in Fig. 2. Two tested journal sliding bearings and a seal rings module were installed on the main shaft. Supporting roller element bearings guided the main shaft in self-alignment housings. The lever system with the ratio 3:1 exerted a radial load (3P) with the weights (P) on the bearings under test through additional ball bearings (marked in orange). This ensured that frictional losses in tested bearings could be measured (assuming that the small friction in the ball bearings can be neglected). Two force sensors with

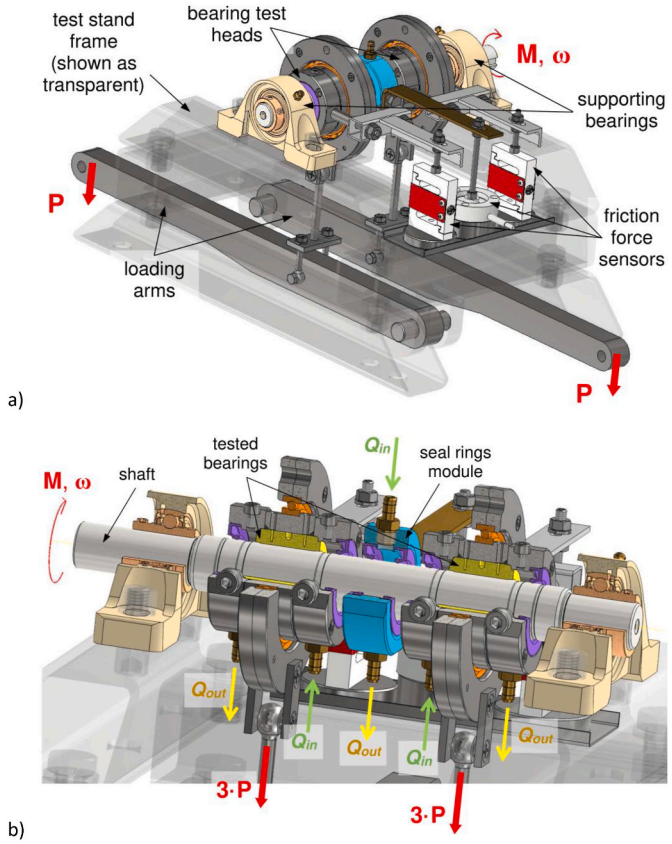

Fig. 2. Tests stand applied for wear tests; a) general view showing friction measurement and loading system, b) detailed view (cross-section).

beams connected to testing bearing heads were used to measure friction losses under operation (see Fig. 2 a)). The measured friction forces were losses in the tested bearing (yellow in Fig. 2 b)) and its sealing (violet colour). Sealing losses were measured using a separate force sensor and a cantilever beam connected to the seal module containing lip seals of the same design as those applied to test heads. This measurement was used as a correction to obtain friction in the tested bearings. During the tests, bearing temperature was monitored using two 1 mm diameter K-type thermocouples. Thermocouples were inserted into blind holes drilled radially close to the bearing ends on its loaded side, with measuring tips positioned 2 mm below the sliding surface (see Fig. 5 a).

A peristaltic pump with a small tank (1 L) equipped with a mixer (to keep the lubricating MR fluid homogenous) was used to feed bearings. The lubricant was pumped separately to both heads (see Fig. 2 b); Q_{in} = 40 mL/min) and the seal module (to ensure similar conditions for the sealing operation). The lubricant was supplied to the heads from one end of the bearing. It flowed axially through the bearings, with two open lubrication grooves (axial) located in the horizontal plane. The lubricant was discharged on the other bearing side and collected in a tank. One wear test consisted of 8600 cycles of start/stop tests with a data recording frequency of 1 Hz (mean value of 1k samples per second). Each cycle lasting 15 s contained forced start-up, steady state operation and free run shutdown.

Since the effect of material on the MR fluid-lubricated bearing system wear process was investigated, bearings produced from different materials were tested. Bronze (CuSn7Zn4Pb7-C) was used as a base material in most tests. In addition, bearings made of a harder material (steel) and softer polymer (compressive modulus of elasticity 2.2 GPa, hardness 83 shore D, melting point 260 °C) and rubber (oil and chemical resistant rubber, hardness 70 ± 3 shore) were also tested. Commercially available bearing sleeves made of polymer and rubber were selected, which are designated for applications that require operation under increased wear conditions. FTIR and TG (in a nitrogen atmosphere) methods were used to determine the composition of the soft bearing sleeves. The results of these measurements (Fig. 3) allowed to identify that the polymer sleeve material was a PPS-based polymer composite, and the rubber sleeve material was a Low-cis Butadiene-based rubber composite. Due to simplicity, they will be referred to further in the paper as polymer and rubber bearing sleeves.

In the case of polymer bearing, intermediate sleeves were used to assemble polymer inserts for tests. The tested rubber bearing had a different design (typical for water-lubricated bearings), with 8 axial grooves evenly distributed on the bearing perimeter. For shaft material, carbon steel (typical for ship shafts) was assumed to be used for all tests. Dimensions of tested bearings, materials and operation conditions were collected in Table 1.

One series of tests focused on the effect of a magnetic field on the wear process. Therefore, 4 mm diameter x 1 mm thick magnets (magnet flux density = 1.03 T) were installed in the tested sleeve 2 mm below the

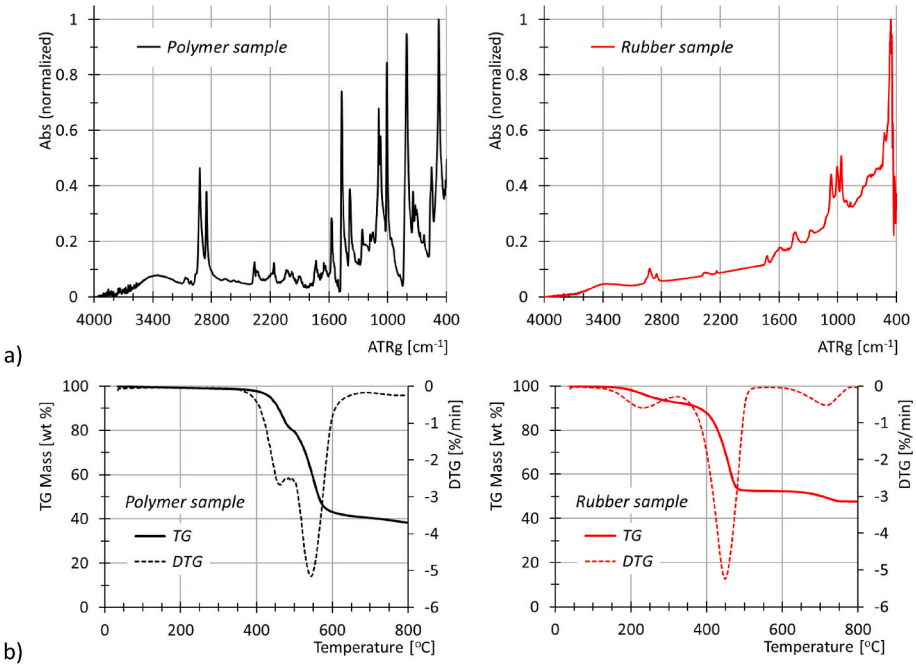

Fig. 3. FTIR (a) and TG and DTG (b) curves of tested bearing material samples.

Table 1
Data on the bearings, materials and operational conditions.

Diameter of the shaft/length of the bearing	30 mm/30 mm
Shaft material/surface roughness	AISI 1045 - Carbon steel/Ra = 0.32 μm
Bearing sleeve material/surface roughness	Bronze CuSn7Zn4Pb7-C/Ra = 0.32 μm Polymer inserts/Ra = 1.25 μm Rubber (8 axial grooves evenly distributed)
Bearing clearance (@ 20 °C)	0.15 mm
Single-cycle shaft speed	Cycle time 15 s 2 s of start-up (0 ↗ 1000 rpm), 10 s of steady-state operation (at 1000 rpm) 3 s of free shut down (1000 rpm ↘ 0) 1 s of time interval between cycles
Radial load (3P) [N]/specific pressure [MPa]	1800 N/2 MPa or 900 N/1 MPa
Friction torque – strain gauge sensor with amplifier, range 0–222 N, nonlinearity ±0.05 % R.O.	
Bearing temperature - K-type thermocouples, accuracy 1.5 K	

sliding surface. They were arranged in two circumferential rows (each composed of 20 magnets) placed close to bearing ends (Fig. 5 a)), and one axial row (composed of 3 magnets) shifted 36 deg from the vertical direction in the vicinity of the expected minimum film thickness zone. The axial row is meant to effectively increases film pressure near the minimum film zone, while the circumferential rows should decrease MR-fluid leakages from the film at the bearing ends, thereby also increasing film pressure. Adjacent magnets were arranged in an alternating order (N – S – N – S – etc.), which, according to numerical analysis [19], results in a magnetic field that is smaller far away from the magnets (relative to the field close to the magnets) compared to a uniform orientation (e.g. N – N – N – N – etc.). This should focus the viscosity increase on the areas of the film directly below the magnets, while limiting the viscosity increase far away from the magnets and thereby reducing the friction losses.

The magnetic field resulting from this arrangement of magnets has been calculated numerically, and is shown in Fig. 4. This calculation was performed using a commercial software package for numerical simulation [36], and other than the bearing geometry (see Table 1) the details of the implementation of the numerical model have been described in detail in a previous paper by the same authors [19].

3.3. Wear amount assessment methodology

The wear assessment of the tested components utilised a comparison of the surface geometry measurements before and after the tests. Measurements were conducted using a contact profilometer (Jenoptik Hommel Etamic T8000, measuring vertical range 400 μm). To compare the profiles before and after tests, both shafts and bearings were

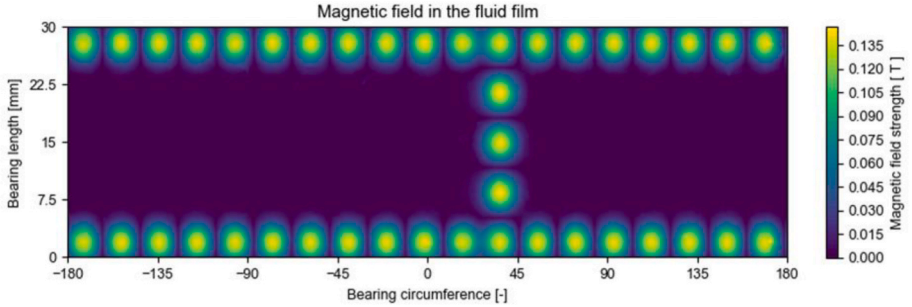

Fig. 4. Tests stand applied for wear tests; a) general view showing friction measurement and loading system, b) detailed view (cross-section).

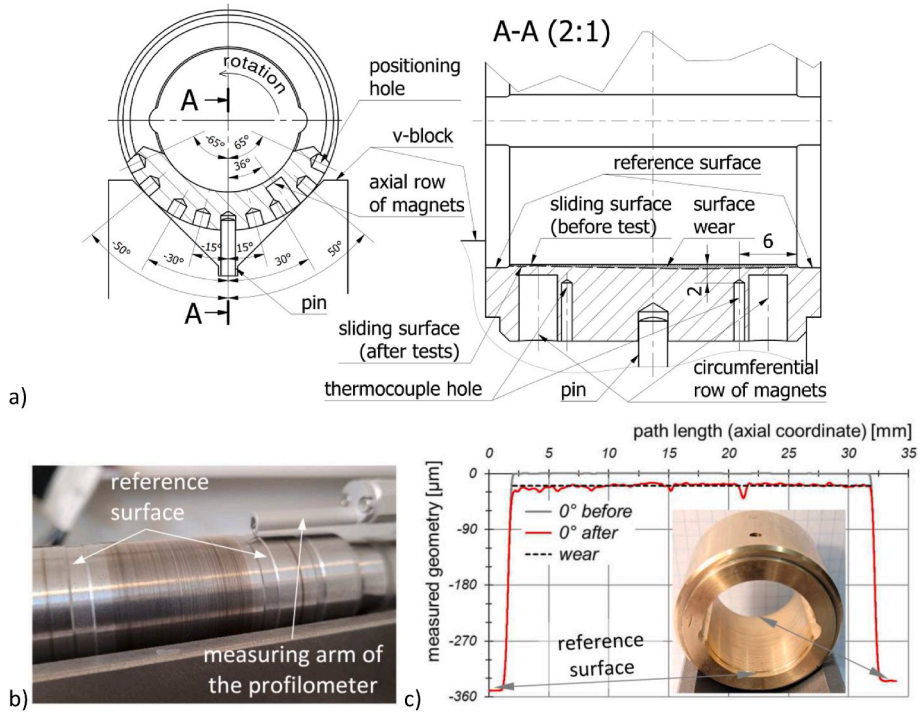

Fig. 5. Sliding surface measurements, a) bearing sleeve; b) shaft; c) an example of measured geometry profiles of sliding surface and linear wear assessment.

manufactured with special reference surfaces in the shape of grooves, with the bottom surface below the sliding surface, to avoid their wear during operation (Fig. 5).

The axial profiles of the mating surfaces started and finished each time at reference grooves. For each sleeve, several axial profiles were measured on the loaded bearing half (evenly distributed to the direction of the load, initially 5 paths in a range ± 30 deg, later 9 paths in a range ± 65 deg, Fig. 5 a). Positioning holes made at the outer surface of the bearing, together with a pin mounted in the v-block groove, provided accurate (and repeatable) angular positions of the bearing for measurements. One axial profile was collected for each shaft journal in marked angular position since differences in measured geometries for other circumferential positions were negligible.

Fig. 5 c) shows an example of a measured sliding surface profile comparison. Since the geometry of the reference surfaces did not change during the wear test, it was possible to compare profiles. The difference in the average level of the sliding surface before and after the wear test was a measure of the linear wear. The same comparison was carried out for each angular position of the sleeve. As a result, a circumferential distribution of wear for the loaded half of the bearing was obtained. This distribution was also used to calculate the volumetric wear of the sleeves, assuming that the sliding surface was unfolded and changes in the wear between measurement points (namely path positions) were linear. In the case of shaft journals, volumetric wear was calculated as a difference in volume between a journal with nominal size (before the test) and one with a radius reduced by linear wear (after the test).

3.4. SEM analysis

A JEOL 6010LA scanning electron microscope (SEM) with integrated energy dispersive X-ray spectroscopy (EDS) functionality was used for two different investigations after the wear tests had been performed. First of all, micrographs of the shaft and bearing surfaces were created to investigate the wear mechanisms, and elemental analysis of the surfaces was performed using EDS to check for possible material transfer between the shafts, bearings, and particles. For this purpose, the shafts and bearings were cleaned by hand with isopropyl alcohol and were cut into smaller pieces, and before being placed in the SEM the non-conductive rubber and polymer bearing surfaces were coated with a thin layer of gold to improve the imaging results.

Secondly, the SEM was used to perform an analysis of the particle sizes before and after the wear tests. In order to extract the particles from the MR fluid, the fluid had to be destabilized using acetone. This was done by adding MR fluid and acetone in a 1:1 ratio to a container, which was placed in a shaker for 1 min. After this minute, the container with the mixture was placed on a large NdFeB magnet, rapidly causing the particles to be pulled towards the magnet and leaving a mixture of acetone, oil, and additives floating on top. With the container still on the magnet the supernatant liquid was decanted, and this process was repeated until the decanted liquid started running clear. After drying, the particles were sprinkled on carbon tape to enable imaging with the SEM, resulting in micrographs containing thousands of particles. Image analysis software with particle analysis functionality [37] was used to find the particle size distribution based on these micrographs. This was done by first applying a median blur filter (blur radius 0.25 µm) to denoise the micrograph, followed by an application of the Li threshold algorithm [38] to separate the particles from the background. Finally, the watershed algorithm was used to separate partially overlapping particles. This sequence of operations was qualitatively found to result in reasonable recognition of the particles by the particle analysis function.

4. Wear test results

During each wear test, two bearing sleeves and one shaft with two bearing journals were tested simultaneously. This allowed us to assess the repeatability of the process by comparing the wear results for components tested separately under the same operating conditions. The results showed that linear wear did not differ significantly between sleeves and journal shafts from one test. Consequently, the linear wear results presented in this section are averaged values obtained for the same component type (sleeve and shaft) in one test.

Wear tests were started for a system with bronze bearings under 2 MPa of specific pressure loading and lubricated with the mineral oil

Castrol MHP 153 (SAE 30) using the same methodology as planned for MR-lubricated bearings. The results obtained from this test were used as reference values to assess the wear resistance of tested components with MR-fluid lubrication. The tests were planned and carried out so that it was possible to analyse the impact of a single parameter of the system on the process of component wear. The research plan covered the test focused on effects of bearing load, MR-fluid type, presence of magnetic field, and bearing material. Obtained results were shown and described in the following parts of this section (4.1–4.4).

4.1. Effect of the load

In the first series of experiments, bronze bearings lubricated with MR 70 % were tested under the same conditions as in the reference case (under load of 2 MPa). At this stage, magnets were not installed in the bearings, so no magnetic field acted on the fluid. The results showed a huge wear of components. Consequently, the next test was planned and carried out with the reduced bearing load (to 1 MPa) to investigate the impact of this parameter on wear under MR-fluid lubrication.

In Fig. 6, a summary of the wear results for load effect under MR-fluid lubrication was presented and compared to results obtained for the reference case (oil-lubricated bearing). Fig. 6 a) presents measured circumferential distribution of linear wear for sleeves (note that results for MR 70 % and 2 MPa load were scaled – reduced by factor 10 - to fit them in the plot). In Fig. 6 b) measured wear for shaft journals and sleeves were compared. The circumferential distribution of the bearing sleeve wear was not symmetrical to the load direction (angular position of 0° in Fig. 6 a)). This shape is typical (visible in all further results), as higher linear wear occurs near the minimum lubricant film thickness zone. Under the load of 2 MPa, the volumetric wear of the bearing and journals lubricated with MR 70 % was two orders of magnitude (!) higher than that of the reference case (Fig. 6 b)). After reducing the load to 1 MPa, the wear of the components lubricated with MR 70 % was also reduced; however, it was higher from 5 (for sleeves) to 7 times (for journals) than in the reference case.

4.2. Effect of the MR lubricant

The measured level of component wear lubricated with MR 70 % fluid was unacceptable in the case of real bearing system operation. One reason for this can be the relatively high concentration of particles in the MR fluid that was applied as a lubricant in previous tests. To investigate the effect of MR lubricant with lower particle content on system wear, a new fluid, MR 20 %, was developed and provided for testing. Wear tests, as previously, were carried out for bronze bearings under the load of 1 MPa.

Fig. 7 shows the measured wear distribution for sleeves (a) and journals (b) lubricated with MR 70 % and MR 20 % fluids compared to the reference case. Surprisingly, the volumetric wear of the sleeves lubricated with the MR 20 % fluid with a lower concentration of the particles was significantly higher (about 60 %) than for MR 70 % lubrication. It was much worse in the case of journals since their wear was an order of magnitude higher than the wear of parts operated with MR fluid with a higher concentration of particles. In addition, it was even slightly higher than shaft journal wear, measured for MR at 70 % under 2 MPa load (see Fig. 6 b)).

4.3. Effect of the magnetic field

Activating the magnetic field (MF) is required to gain the unique benefits of MR lubrication (change of the lubricant viscosity and thus adjustment of bearing properties—active bearing principle). One of the tests evaluated the effect of MF presence on the bearing system components' wear. The test was carried out using bronze bearings with magnets assembled in the bearing body (as described in paragraph 3.2) and for a load of 1 MPa.

Fig. 8 shows the measured wear results for the bearing system components lubricated with MR 70 % fluid with activated MF compared to the case without activated MF. The volumetric wear of the shaft journals was found to be higher while the MF was activated (less than 2 times higher). Simultaneously, the level of volumetric wear for the bearing sleeves operated with and without the magnetic field was the same. However, the angular wear range was slightly narrower (shorter) when the system was tested without an activated magnetic field.

4.4. Effect of the material

Parameter changes studied and described in previous parts of this chapter did not cause a reduction of the system component's wear lubricated with MR-fluid to a level similar to that observed for the reference case. The last of the studied parameters was the material of the bearing. Different types of materials were tried, with varied properties. One of them was steel, whose hardness is much higher than bronze, which was expected to be beneficial for wear reduction. However, tests with steel bearings lubricated with MR 70 % fluid under the load of 1 MPa failed catastrophically after several start/stop cycles, probably due to scuffing and the effect of having the same material for both mating surfaces. Thus, no results were available for this test.

In further tests, softer materials, such as polymer and rubber, were used. Polymer bearings tested were cylindrical plain bearings of the same design as tested bronze bearings. In the case of rubber bearings, due to the lack of availability of a design and size similar to the tested one, a typical design for water lubrication with 8 axial grooves distributed evenly around the bearing perimeter was tested. Tests were carried out under the load of 2 MPa and with MR 70 % as lubricant.

Fig. 9 shows the wear results for different tested materials of the bearing sleeve. Since a reference surface could not be manufactured on the rubber bearings (the rubber was too soft, later on this also prevented accurate profile measurements with the profilometer), the proposed wear measurement method could not be used. Other wear assessment

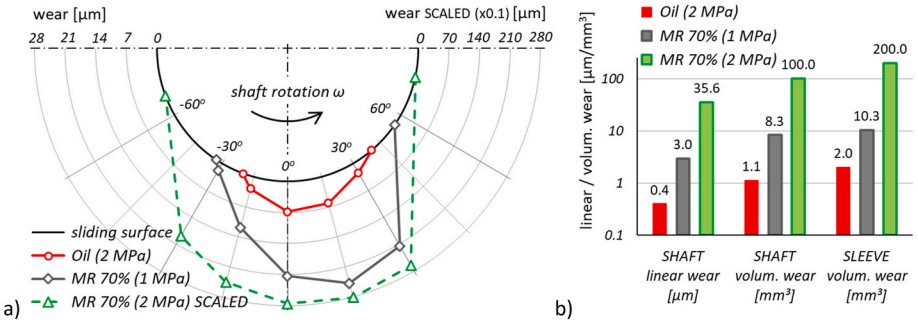

Fig. 6. Effect of the load on the wear of bearing components lubricated with MR fluid: a) distribution of the linear wear at the circumference of the sleeves, b) linear wear of the shaft journals and volumetric wear of the sleeves and shafts.

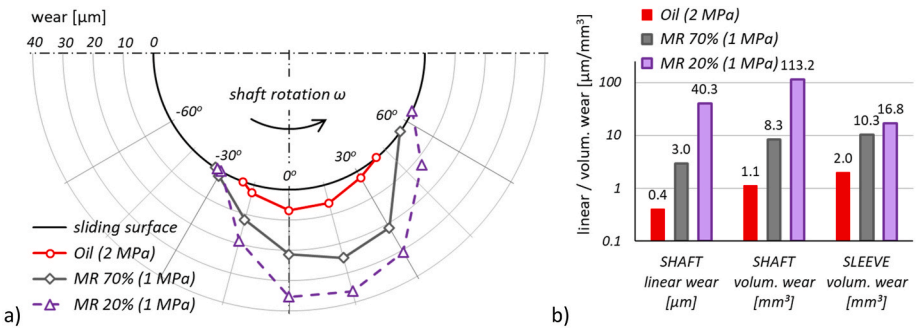

Fig. 7. Effect of the MR fluid type on the wear of bearing components: a) distribution of the linear wear at the circumference of the sleeves, b) linear wear of the shaft journals and volumetric wear of the sleeves and shafts.

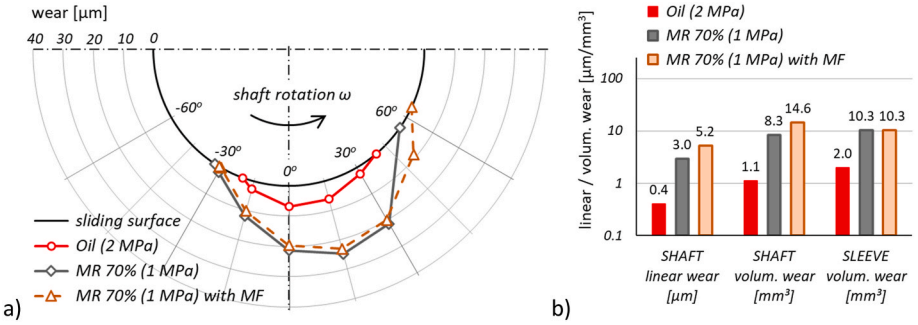

Fig. 8. Effect of the magnetic field (MF) on the wear of bearing components lubricated with MR fluid: a) distribution of the linear wear at the circumference of the sleeves, b) linear wear of the shaft journals and volumetric wear of the sleeves and shafts.

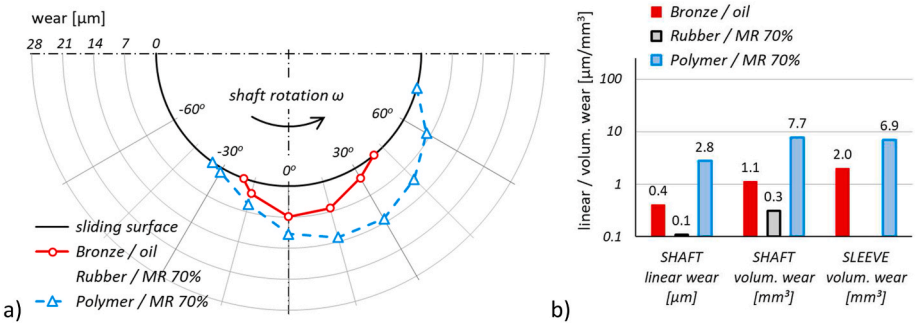

Fig. 9. Effect of the sleeve material on the wear of bearing components lubricated with MR fluid under the load of 2 MPa: a) distribution of the linear wear at the circumference of the sleeves, b) linear wear of the shaft journals and volumetric wear of the sleeves and shafts.

methods were considered for rubber bearings, such as the weight method or employing a Coordinate Measuring Machine (CMM); however, their accuracy was not satisfactory considering the level of wear on the components. Thus, the wear amount of the rubber bearings could not be determined.

The polymer volumetric wear was higher than the reference value for oil-lubricated bearings. However, the wear on polymer bearings was the smallest among all wear tests with MR fluid lubrication. In the case of the shaft, the wear of the journals operated against the polymer was higher than the reference (around seven times). Simultaneously, the volumetric wear of the journals after tests with rubber bearings was hardly measurable and even smaller than for oil-lubricated bearings.

4.5. Coefficient of friction (COF) and temperature

In Fig. 10, the measured coefficient of friction (COF) obtained during all wear tests reported in this paper is compared (for both bearing sleeves tested simultaneously during a given test). The values shown in the figure are the average values of the bearing friction coefficient (considering the seal friction correction) for all start/stop cycles at the end of steady-state operation of the bearing with a speed of 1000 rpm (fluid friction mode, approximately 12 s for each cycle assuming that typical cycle consists of 2 s acceleration from standstill to the nominal steady state velocity that is maintained for 10 s, followed by a deceleration again to zero velocity in 3 s, Table 1). This choice was motivated by the relatively low frequency of the signal recording applied in this research, which did not allow for monitoring the evolution of the COF during transient states of bearing operation (start-up and shut-down). In addition, while both bearings operated with the same shaft, they had some impact on each other during the start and stop of the bearing system which was not the case during steady-state operation. In addition, Fig. 10 shows the standard deviation of the COF (as error bars calculated using all 8600 data points), which enables the assessment of friction variability in the bearing during tests.

The results in Fig. 10 show that the smallest values of COF and their standard deviations were measured during the test with the oil as a

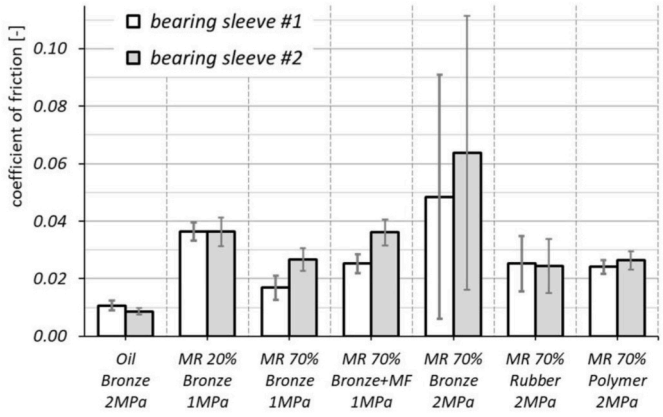

Fig. 10. Comparison of the coefficient of friction for both bearing sleeves tested during a given wear test with standard deviation bars (calculated using 8600 data points).

lubricant at the load of 2 MPa (reference case), while the highest friction was noticed for MR 70 % and 2 MPa. This last case also showed the largest difference in the average friction coefficients between the two tested bearings, as well as the largest standard deviations, meaning significant variability of the COF during tests. A much lower COF was measured under MR 70 % lubrication when the load was reduced from 2 to 1 MPa. However, it was still higher than for the reference case (over 2 times). It can be noticed that the COF measured for MR 70 % was lower than for MR 20 % (at the load of 1 MPa) and that the activated magnetic field also increased the measured COF compared to the case without MF (for MR 70 % and 1 MPa). When compliant and soft materials (rubber and polymer) were applied for bearing sleeves, the measured friction coefficient was similar and equal to ~0.025. It was, however, still higher than in the reference case (around 2.6 times).

Results of the bearing temperature during tests showed no significant changes for most of the cases. The measured temperature varied only slightly during the entire test, keeping a constant level around 35–45 °C. The lowest temperature was measured in the polymer bearing; however, due to the low thermal conductivity of this material, it cannot be compared directly to the measurements for metallic bearings (bronze). On the other hand, high temperature variations were noticed for MR 70 % bronze bearing tested under the load of 2 MPa. In this case, the

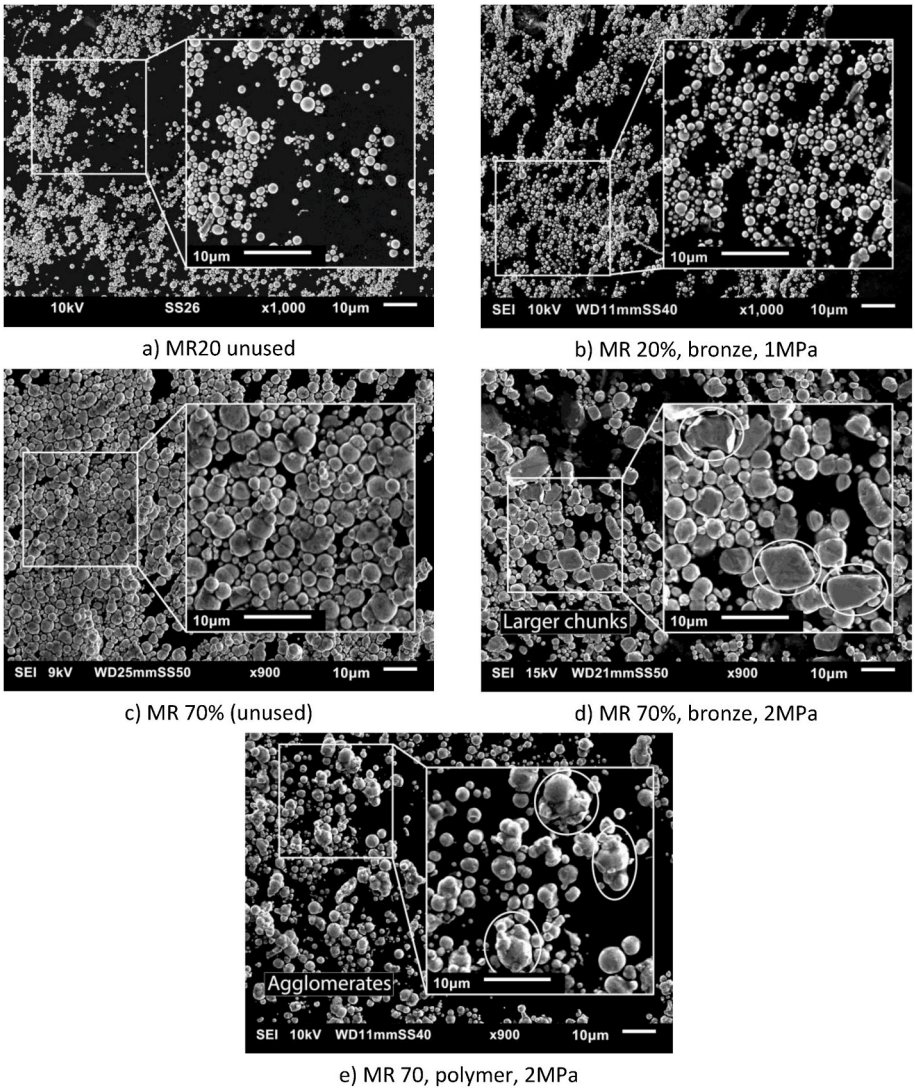

Fig. 11. SEM micrographs of particles taken from several MR fluid samples. In subfigure b) several larger chunks of iron are encircled, and in subfigure c) the same is done for several particle agglomerates. Note that the micrographs in subfigures c), d), and e) were taken with an SEM magnification of 900x as indicated in the figures, but that these were zoomed in digitally to 1000x to match subfigures a) and b).

measured temperature course was "chaotic". It showed variations in a relatively large range (45–95 °C), which was caused by periodic bearing operation with high friction (periods with the higher friction torque in the bearing correspond to higher bearing temperature).

4.6. Particle size analysis before and after start/stop tests

A particle size analysis was performed for samples of the MR fluids collected after the wear tests described in sections 4.1–4.4 and for samples of the unused MR 20 % and MR 70 % fluids. Micrographs of the particles from these samples were analysed with image processing software to determine the particle size distributions, but before these distributions are discussed, a qualitative comparison of the particle shapes and sizes will be made using several representative micrographs. The effectiveness of the image analysis procedure for each of these micrographs will also be discussed.

4.6.1. Qualitative analysis

Fig. 11 shows five of these micrographs, representing groups of particle samples with distinct properties.

The first group contains the MR 20 % samples, both before and after the wear test, and is represented by Fig. 11 a) and b). As can be seen in the figures, the particles in this group are round and there are hardly any particle agglomerates. The image analysis procedure described in section 3.4 was found to work very well for this group.

The second group consists only of the samples collected after the wear tests with a bronze bearing loaded to 2 MPa and lubricated with MR 70 %, and is represented by Fig. 11 d). As can be seen in Fig. 6, the wear of both the shaft and the bearing was very high during this wear test, and it is clear that the particles were also damaged. Compared to the first group, and to the particles from the unused MR 70 % fluid shown in Fig. 11 c), the particles from this group are generally less round and their surfaces are less smooth. Furthermore, several large non-round chunks of iron can be found between the particles (some have been encircled in Fig. 11 d), these were probably created when individual particles were flattened or crushed together in the contact zone of the bearing. For this group the image analysis procedure works well too.

The final group includes all remaining MR 70 % samples, and is represented by Fig. 11 e), where the particles collected after one of the polymer bearing tests are shown. The micrograph shows that the individual particles are still mostly round, but that there are also quite a few agglomerates consisting of multiple particles sticking together which were not present in the unused fluid from Fig. 11 c) (some of these have been encircled in the figure). In contrast to the heavily worn particles from Fig. 11 d), these agglomerates still recognisably consist of individual particles.

As a result, the particle analysis procedure was observed to frequently find the individual particles making up these agglomerates, instead of considering an agglomerate itself as one single particle. Whether or not the image analysis was successful seemed to depend on the brightness and contrast of the agglomerate surface on the micrographs, specifically in those regions where the individual particles making up the agglomerates touch. It is therefore expected that the particle size distributions created for the fluid samples containing these types of agglomerates will underestimate the amount of relatively large particles, and will overestimate the number of small to medium particles.

4.6.2. Particle size distributions

Fig. 12 contains the particle size distributions for all MR fluid samples. As was mentioned in section 3.1, a different batch of (smaller) particles was used for the MR 20 % fluid, explaining the stark difference in the distributions of the MR 20 % and MR 70 % fluids. There is also very little difference between the distributions before and after the MR 20 % wear tests, which matches the qualitative analysis. Continuing to the MR 70 % tests, it can be seen that the difference in the distributions

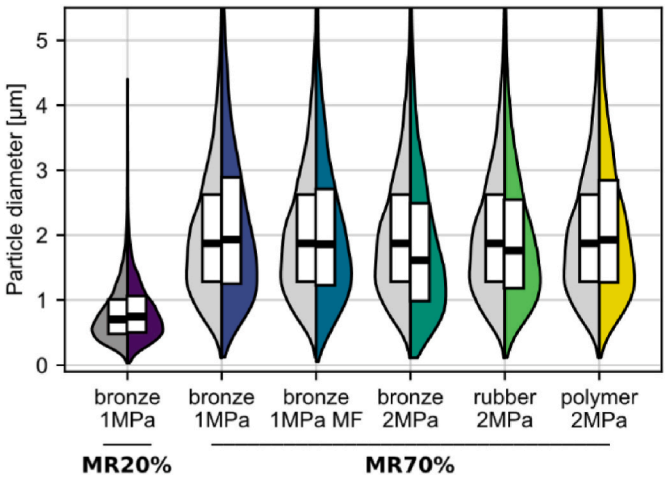

Fig. 12. A violin plot of the particle size distributions both before and after the various wear tests. All violins have been calculated by combining the particle size data obtained from three different micrographs, all containing at least 1000 particles from the same MR fluid sample. The left (greyscale) side of every violin represents the unused MR fluid, the right (colored) side represents the MR fluid after the wear tests. The box plots inside the violins show the first and third quartiles, as well as the medians.

before and after the wear tests is small for most of these samples as well. The largest difference can be observed for the bronze bearing lubricated with MR 70 % and loaded to 2 MPa, where the first quartile and median have both decreased by about 0.26 µm after the wear test, and the third quartile has decreased by about 0.11 µm. This corresponds with the qualitative analysis, where it was observed that this was the only wear test where the particles themselves seemed to have been damaged (see Fig. 11 b)).

Lowering the load to 1 MPa prevents the particles from being worn down as much, with the first quartile and median changing no more than 0.1 µm. The third quartile does increase by about 0.26 µm, which could indicate an increase in the number of particle agglomerates that have been formed. Interestingly, this increase is not visible when the magnetic field is activated during the wear test. Finally, for the rubber bearing there is little difference in the size distributions before and after, with only a small decrease of all quartiles by less than 0.1 µm after the test. In contrast, the polymer bearing shows a similar increase of the third quartile as was observed with the bronze bearing loaded to 1 MPa (though the polymer bearing was loaded to 2 MPa).

4.7. Surface analysis

SEM micrographs were made of the surfaces of the bearings and shafts used during the wear tests, to help explain the wear mechanisms occurring with MR lubrication. Fig. 13 shows these micrographs for all bronze bearings, the micrographs of the corresponding shafts are only shown for the reference case (oil lubrication) and for the MR-lubricated cases with high shaft wear (MR 70 % with 2 MPa and MR 20 % with 1 MPa). All other shaft micrographs were qualitatively found to be indistinguishable from the reference case. Fig. 14 shows micrographs of the surfaces of the softer rubber and polymer bearings that were tested. Of the shafts, only the micrograph of the shaft used with the rubber bearing is shown, the shaft used with the polymer bearing was lost in transit between two labs. Finally, the sliding direction was upwards in all micrographs, and the micrographs of the bearing surfaces were taken at the bottom of the bearing, in the contact zone, unless mentioned otherwise.

4.7.1. Bronze bearings

The unused and used bearing surfaces of the bronze bearing

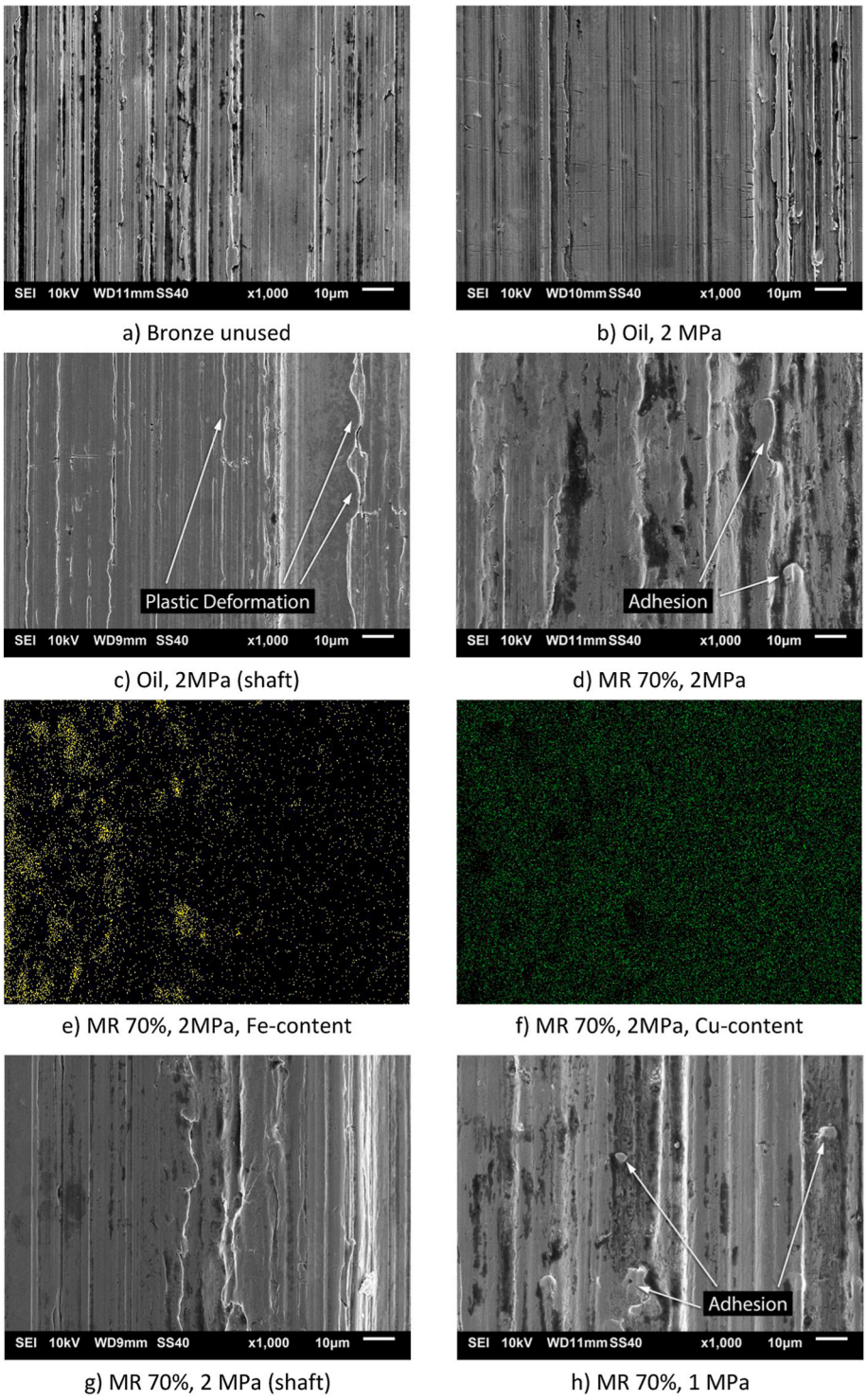

Fig. 13. SEM micrographs and EDS maps of several bronze bearing surfaces for various operating conditions, as well as some representative steel shaft surfaces. The sliding direction was upwards in all cases.

lubricated with oil are shown in Fig. 13 a) and 13 b) respectively. The unused surface contains many ridges in the vertical direction left by the original machining process, and while several ridges have worn down after the wear test, some of these marks are still visible on the right side of the micrograph of the worn surface. The condition of the worn shaft surface looks similar to that of the bearing surface, though some plastic deformation of the ridges can also be seen (Fig. 13 c)).

With MR lubrication, the appearance of the surfaces changed dramatically after the wear tests. Fig. 13 h) and 13 d) show the bearing micrographs for loads of 1 and 2 MPa respectively, and at first glance their overall appearance is similar. For both loads the original machining marks have disappeared completely, almost certainly due to large amounts of third body abrasive wear caused by the particles. Furthermore, several features are visible that indicate that some adhesive wear may have occurred. Next to that, Fig. 13e) and 13 f), which represent EDS maps of the iron and copper content, show large patches

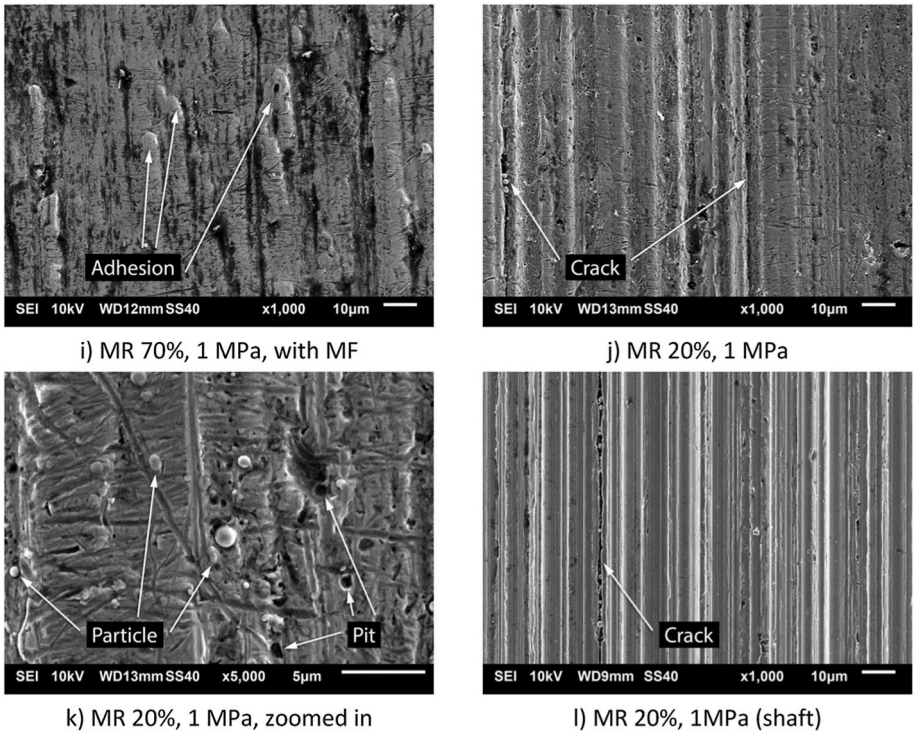

Fig. 13. (*continued*).

of (pure) iron on the surface of the bearing loaded to 2 MPa, while no iron could be found on the surface of the bearing loaded to 1 MPa. Finally, the shaft used with the bearing loaded to 2 MPa is shown in Fig. 13 g). Its surface looks very similar to that of the oil-lubricated shaft (Fig. 13 c)), but there seems to be some cracks running in the sliding direction.

In the next wear test, magnets were added to the MR lubricated system loaded to 1 MPa, resulting in the micrograph in Fig. 13 i) which was taken at a location on the surface directly above one of the magnets. The overall appearance of the surface is the same as it was without the magnets present, apart from a large number of small scratches.

Finally, Fig. 13 j) and 13 l) show the effect of a reduced particle concentration (20 % by volume) on the surfaces of the bearing and shaft respectively. The contrast with the other micrographs for the bearings lubricated with MR 70 % is large, with both the bearing and shaft surfaces containing some cracks, and the shaft surface showing many ridges in the sliding direction. When zooming in on the bearing surface (Fig. 13 k)) it can be seen that this surface is heavily scratched and contains many embedded particles. Furthermore, many pits can be found in the surface, some of which are almost perfectly round, indicating that a number of embedded particles may have been dislodged during the wear test. Similar to the MR 70 % test with a load of 1 MPa, no iron could be found in the bearing surface itself (apart from the embedded particles).

4.7.2. Rubber and polymer bearings

Starting with the rubber bearing, Fig. 14 a) and 14 b) show the surface before and after the wear test respectively. While it was not possible to determine the volumetric wear of the rubber bearing, the micrographs do indicate that the appearance of the surface has at least changed drastically. The original machining marks (horizontal ridges that were left by the molds) have worn away completely, and the surface instead contains vertical grooves, as well as some pits. Particles are visible in some of these pits, and individual particles have been embedded in the rubber as well in some other locations.

In contrast, the surface of the corresponding shaft shown in Fig. 14 c) does not show major signs of wear, and looks similar to the lightly worn shaft used in the oil-lubricated bronze bearing (see Fig. 13 c)). Only some fine scratches are visible, which are probably caused by particles embedded in the rubber. These results agree with the linear wear tests, which showed minimal wear of the shaft (see Fig. 9). The remaining figures all show micrographs and EDS maps for the polymer bearing surface (unfortunately the shaft used for the polymer bearing test was lost during shipping between the participating research groups). This was the only bearing where a clear difference could be observed in the appearance of the surface in the converging region of the film, compared to the surface close to minimum film, which is why micrographs were made of both regions of the bearing.

Starting with Fig. 14 d), the unused polymer surface shows very obvious machining marks, with clear vertical ridges about 100 μm apart, and smaller, regularly spaced horizontal grooves in between. This texture is still visible on some parts of the worn surface in the converging region of the film, as can be seen in Fig. 14 e), but large clumps of iron have also been smeared onto the surface, forming an almost continuous layer of iron on top of the polymer. This becomes even more obvious when zooming in (see Fig. 14 g)) and comparing the micrograph with the EDS maps for iron and carbon (Fig. 14 i) and 14 j) respectively, with carbon being the main element of the polymer). The diverging half of the bearing has a very different surface, as can be seen in Fig. 14 f). The mostly continuous layer of iron from the converging region tapers off into smaller branches in this region. Furthermore, the original machining marks have been worn away completely and there are obvious grooves and ridges in the sliding direction. When zooming in on one of the areas without a layer of iron (see Fig. 14 h)) and comparing the micrograph with the EDS maps for iron and carbon (Fig. 14 k) and 14 l), respectively), it becomes clear that there is still a large amount of iron on the polymer bearing surface, mostly in the form of smaller clumps and individual particles embedded in the surface.

5. Discussion

The comprehensive research program allowed us to investigate different aspects of the tribological properties of the system lubricated

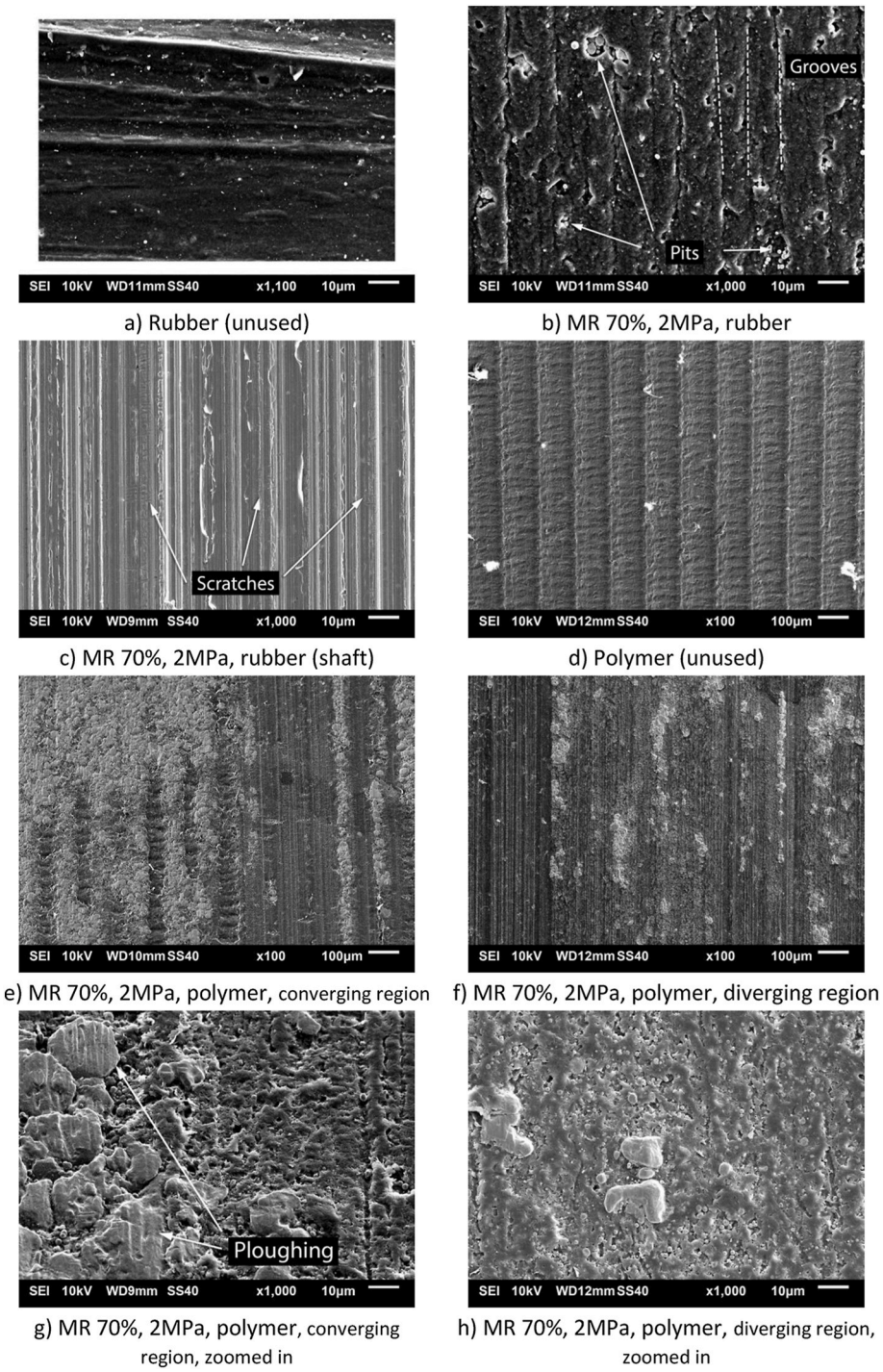

Fig. 14. SEM micrographs and EDS maps of the rubber bearing surfaces (subfigures a) through c)) and polymer bearing surfaces (subfigures d) through l)). The sliding direction was upwards in all cases. Note that the micrograph in subfigure a) was taken with an SEM magnification of 1100x as indicated in the subfigure, this micrograph was zoomed out digitally to 1000x to match the other subfigures.

with the MR fluid and compare the obtained results to those of an oil-lubricated bearing tested under the same conditions. This section discusses the results presented in the previous sections of the paper.

The oil-lubricated bearing sleeves and shaft journals (reference case) showed low friction coefficients and relatively small amounts of wear under the load of 2 MPa (Fig. 6), which agrees with the very minor differences in the surface micrographs before and after the wear tests (Fig. 13 a) through c)). In contrast, the wear of the mating components was found to be higher (sometimes much higher) in most of the tested bearing configurations lubricated with MR fluid. The bronze bearing lubricated with MR 70 % under a load of 2 MPa showed the highest wear, which was found to be two orders of magnitude higher (!) than in the reference case. The friction coefficient was also found to be 5.5 to 6 times larger for steady-state operation (Fig. 10), which could indicate permanent mixed or boundary lubrication, especially since the standard deviation on the friction measurements was high as well for these tests. As was to be expected, these extreme levels of wear and friction could be reduced by lowering the load to 1 MPa, but even then, they were still

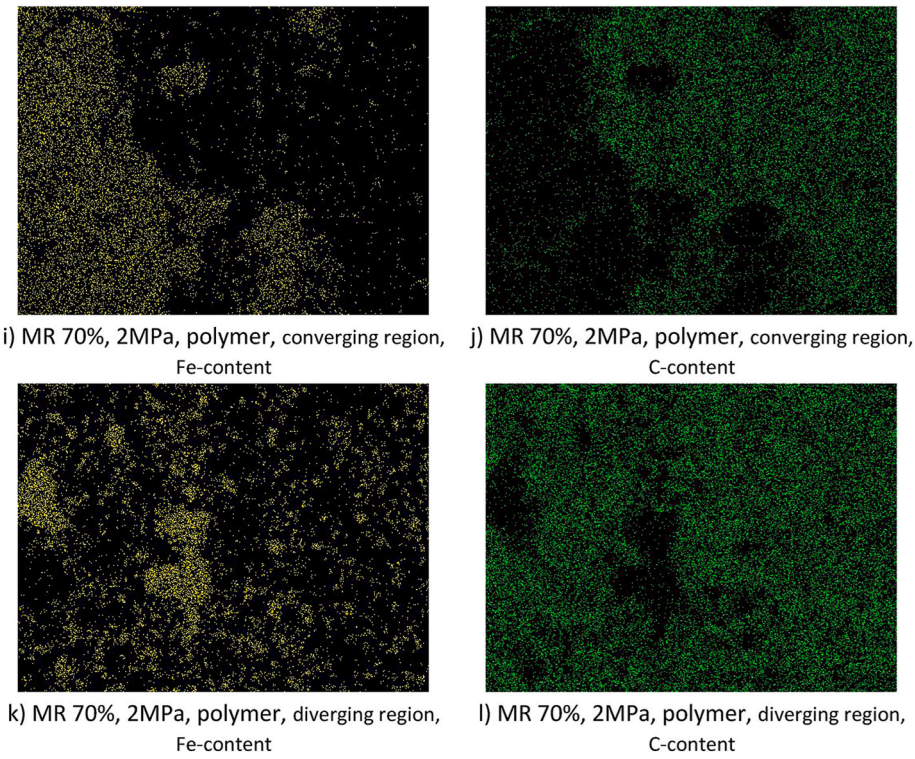

Fig. 14. (*continued*).

several times higher than for oil-lubricated bearings. For both loads the large amounts of wear are probably the result of third body abrasion, however, looking at the micrographs of the mating surfaces (Fig. 13 d) through h)) also reveals some differences in the wear mechanisms for these two load cases. As was observed in the results section, the bronze sleeve surface of the bearing loaded to 2 MPa contained patches of pure iron, while this was not the case for the lower load. The only two components in the bearing system containing any iron were the particles (pure iron) and the shaft journal (AISI 1045 carbon steel). Since the EDS did not detect any elements in these patches other than iron (such as manganese, which appears in AISI 1045), these patches can only consist of (the remains of) particles. It seems likely that with the higher load of 2 MPa, particles were flattened or crushed into the bearing surface and were then worn down together with the bronze, since the areas on the EDS map that contain iron do not match up with the ridges visible on the micrograph (Fig. 13 e) and d) respectively). Since no patches of iron were found with a load of 1 MPa, it seems likely that this load was too low to cause such a deformation of the particles. This difference was also revealed by the particle size analysis in section 4.6, where it was found that only the particles from the bearing loaded to 2 MPa were visibly worn (Fig. 11 d)) and had decreased in size after the wear test, while the particles from the bearing loaded to 1 MPa had roughly the same size before and after (Fig. 12).

The effect of the magnetic field was much smaller than that of bearing load. The friction increase compared to the reference went up from 2.3 times without magnetic field to 3.2 times with magnetic field (Fig. 10), which was caused by the magnetically induced viscosity increase. With the activation of the magnetic field the wear of the shaft journals was also slightly higher than without a magnetic field, but the wear of the bearing sleeves did not change (Fig. 8). This could be caused by the formation of particles chains at the locations of the magnets that are embedded below the stationary bearing sleeve surface. These chains will mostly stay in position over the magnets [39], likely causing their ends to be dragged along the surface of the rotating shaft journal. The existence of such a wear mechanism is supported by the fact that only the shaft wear changed with the activation of the magnetic field, the level of wear of the bearing sleeves remained the same. The sleeve surface micrographs did show a large number of scratches though (Fig. 13 i)), these may have appeared during the transitions to boundary lubrication, with the magnetic field pinning the particles near the magnets in the contact zone in place, preventing them from moving along with the rotating shaft. Such an effect could also be the cause of the reduction of the number of agglomerates consisting of multiple particles compared to the unactivated bearing (Fig. 12).

In contrast to initial expectations based on literature about lubrication experiments with contaminated water [40,41], a reduction in the particle concentration from 70 % to 20 % did not lead to lower wear, but actually increased wear. The amount of wear noticed for the bearing sleeves was only slightly higher (around 60 %, see Fig. 7), but the shaft journal wear increased by a significant amount (an order of magnitude) with MR 20 % lubrication compared to wear results for the standard MR fluid (MR 70 %, 1 MPa). Compared to that bearing the friction coefficient also increased slightly. An explanation for these wear results might be found by examining the surface micrographs (Fig. 13 j) and 13 l)). As was mentioned in the results section, the shaft journal surface was heavily grooved in the sliding direction, while the bearing sleeve surface contained many embedded particles. However, unlike the 2 MPa MR 70 % test there were no patches of iron in the sleeve surface meaning that the particles were not crushed or flattened into the surface like they were at that higher load. Similarly, the particle size analysis indicated barely any change in both the size and shape of the particles in the MR 20 % fluid before and after the wear tests (Fig. 12). Taken all together, it seems likely that the qualitative information from the manufacturer (section 3.1) was correct, and the hardness of the particles in the MR 20 % fluid was indeed higher than of those in the MR 70 % fluid. The exact difference in hardness between the MR 20 % and MR 70 % particles is not known, and it was found to be difficult to measure the hardness due to the extremely small size of the particles.

Do note that there could also be an alternative explanation for the difference in particle hardness between the two MR fluids. Work hardening of particles has been observed in literature [27,28], and it is possible that the lower concentration of 20 % led to higher stresses on

the individual particles. However, since the deformation of the particles seems to have been minimal, it is deemed more likely that the particles in MR 20 % did indeed have a higher hardness to begin with, but this could be investigated further.

The results for the tests with the bearings made of compliant materials show very different results compared to the bronze bearing. Both polymer and rubber bearings show a comparatively modest increase in friction coefficient by about 2.6 times (Fig. 10). At the same time, the polymer bearing has the lowest bearing sleeve wear level out of all bearings lubricated with MR fluid, and was relatively close to the reference case for both bearing and journal wear (Fig. 9). The wear level on the shaft journal used with the rubber bearing was the lowest of all bearings that were tested, lower even than in the reference case. However, since the sleeve wear could not be measured for the rubber bearing, it is difficult to say anything about its overall wear performance. Looking at the rubber surface micrographs also shows large changes in the surface geometry before and after the wear tests (Fig. 14 a) and b) respectively). The wear to the rubber sleeve surface was at least large enough to completely remove the original machining marks, and to create several grooves and pits that contain particles. These findings match with literature for rubber bearings lubricated with oil or water containing hard particles [40,42,43]. It has been stated that once the oil film becomes thin enough (due to lowered speed or increased load), individual particles with diameters larger than the film thickness will bridge the gap between the mating surfaces. Due to the elasticity of the rubber, the particles will locally deform this surface and will start to roll on the harder shaft surface, minimizing the wear to both components. However, once the system reaches boundary lubrication, the particles will be pressed almost fully into the rubber, which can lead to ploughing of the rubber surface and the formation of furrows or grooves in the sliding direction, similar to those observed in the micrograph. At the same time, local stress concentrations due to the particles deforming the rubber can cause the stress to exceed the strength limit, causing particles to be embedded in the rubber, and leading to the formation of pits [43]. These pits can be identified by the particles that have been collected in them and can be found on the micrographs of the rubber bearing sleeve.

The micrographs for the polymer bearing show that the wear mechanisms for that system differed significantly from those with the rubber bearing (Fig. 14 d) through f)). The polymer bearing sleeve was the only sleeve with a difference in the appearance of the converging and diverging areas of the bearing, with the converging area showing a layer of iron clumps on top of the polymer surface, while the diverging area showed more wear and showed embedded individual particles and smaller clumps. During operation of the bearing, the particles were probably crushed in the converging region of the film, leading to iron clumps that are tens of micrometers wide, much larger than the particles from the fluid which had a median size of 1.9 μm after the wear test (see Fig. 12). Similar to the bronze bearing tested at 2 MPa with MR 70 %, the iron on the bearing surface has been worn during the test, as evidenced by the clear ploughing marks in the sliding direction that are visible on most of the clumps in Fig. 14 g). An obvious difference with the bronze bearing sleeve is that the iron on the polymer surface has formed clearly distinguishable clumps lying on top of the polymer, and has not been smeared out over the sleeve surface (Fig. 13 d)). This may be the result of the lower stiffness and hardness of the polymer bearing, which can deform elastically under load, possibly preventing the particles from being flattened entirely. It could also explain why the average size of the particles in the fluid increased slightly, instead of decreasing like with the bronze bearing sleeve. Furthermore, the resulting layer of iron seems to have partially protected the underlying polymer surface, since the machining marks are still visible through gaps in the iron layer while they have been worn away in the areas without any iron clumps at all. This seems to be a similar effect to what was observed by Leung et al. [28], who found a protective layer of flattened particles on the block of a block-on-ring tribotester lubricated with an MR fluid. They also found that the protective layer did not extend into the diverging region, which is the case for the bearing in this paper as well and would explain the larger degree of visible wear in the micrographs of that region. The individual clumps or iron found in the diverging region are likely wear debris from the iron layer in the converging region.

6. Conclusion

In this research, the wear properties of an MR-lubricated hydrodynamic journal bearing system have been investigated experimentally with start/stop wear tests under varying operating conditions. These results have been compared with a reference, an oil-lubricated bearing with a bronze sleeve, with the aim of finding a bearing sleeve material with a similar level of wear for MR lubrication as that of the reference for oil lubrication. The key conclusions of this investigation are:

1. The wear performance of a standard combination of a bronze bearing sleeve and steel shaft journal is extremely poor for all operating conditions, with an increase in wear of two orders of magnitude compared to the reference, as well as 5 to 6 times increase in friction. The wear increase is likely the result of third body abrasion due to the presence of iron microparticles in the MR fluid (which were also damaged), and could only be reduced by lowering the load applied to the system.
2. Lowering the particle concentration of the MR fluid from 70 % to 20 % did not yield the expected wear reduction but actually increased the wear. The exact reason for this is not known but may be related to an unintended difference in particle size and hardness between the particles in the two MR fluids.
3. Using a rubber bearing sleeve resulted in minimal wear to the shaft journal, reducing it below even the level of wear of the reference, as well as a doubling of the friction coefficient. However, due to the softness of the rubber compound it was not possible to measure the sleeve wear with the profilometer, and the SEM micrographs did reveal some visible damage to the rubber surface. Due to the low level of shaft journal wear it is recommended to further investigate the wear performance of rubber bearing sleeves for MR lubrication.
4. The lowest level of bearing sleeve wear for MR lubrication was obtained with a polymer sleeve, the wear of this sleeve was only ~3.5 times larger than with the reference, while the friction was ~2.6 times higher. It was found that a layer of crushed iron particles had formed in the converging region of the bearing, possibly protecting the underlying polymer. For these reasons, polymer seems like a promising sleeve material for an MR-lubricated bearing operating in low-speed conditions. This has since been reconfirmed by another investigation, where the authors experimentally tested the hydrodynamic performance of an MR-lubricated polymer bearing for a wide range of speeds [44].

CRediT authorship contribution statement

Michał Wodtke: Writing – review & editing, Writing – original draft, Visualization, Investigation, Data curation, Conceptualization. **Wojciech Litwin:** Writing – review & editing, Supervision, Methodology, Funding acquisition. **Gerben van der Meer:** Writing – review & editing, Writing – original draft, Visualization, Methodology, Investigation. **Ron van Ostayen:** Writing – review & editing, Supervision, Methodology, Funding acquisition.

Declaration of competing interest

The authors declare that they have no known competing financial interests or personal relationships that could have appeared to influence the work reported in this paper.

Acknowledgements

This research is funded and supported by Bifröst Research & Development - part of the AEGIR-Marine group. Contact person: D. Nahuijsen – Manager Technology & Innovation.

Data availability

Data will be made available on request.

References

[1] G. Yang, J. Pan, D. Wang, A review on the magnetorheological materials and applications, Int. J. Appl. Electromagn. Mech. 75 (2024) 407–443, https://doi.org/10.3233/JAE-230195.
[2] C.S. Maurya, C. Sarkar, Magnetorheological fluids: a comprehensive review of operational modes and performance under varied circumstances, Rheol. Acta 63 (2024) 765–785, https://doi.org/10.1007/s00397-024-01470-y.
[3] K. Nagaya, A. Suda, H. Yoshida, Y. Ohashi, H. Ogiwara, R. Wakamatsu, MR fluid viscous coupling and its torque delivery control, Tribol. Int. (2007), https://doi.org/10.1016/j.triboint.2006.02.059.
[4] F. Bucchi, P. Forte, F. Frendo, R. Squarcini, A magnetorheological clutch for efficient automotive auxiliary device actuation. Frat. Ed Integrita Strutt, 2012, https://doi.org/10.3221/IGF-ESIS.23.07.
[5] M. Asadi Varnusfaderani, M. Irannejad Parizi, M. Hemmatian, A. Ohadi, Experimental parameters identification of a flexible rotor system equipped with smart magneto-rheological bearing, Mechatronics (2022), https://doi.org/10.1016/j.mechatronics.2022.102880.
[6] L. Wu, X. Dong, B. Yang, Performance enhancement of a rotary magnetorheological damper induced by needle roller structure, Tribol. Int. 201 (2025) 110204, https://doi.org/10.1016/j.triboint.2024.110204.
[7] R.K. Singh, C. Sarkar, Tribological and braking performance study of additive-based MR fluids in shear and hybrid mode using MR drum brake, Tribol. Int. (2024), https://doi.org/10.1016/j.triboint.2024.109284.
[8] P. Turabimana, J.W. Sohn, Optimal Design and Control Performance Evaluation of a Magnetorheological Fluid Brake Featuring a T-Shape Grooved Disc, Actuators, 2023, https://doi.org/10.3390/act12080315.
[9] I.F. Santos, Controllable sliding bearings and controllable lubrication principles-an overview, Lubricants (2018), https://doi.org/10.3390/lubricants6010016.
[10] Ł. Breńkacz, Ł. Witanowski, M. Drosińska-Komor, N. Szewczuk-Krypa, Research and applications of active bearings: a state-of-the-art review, Mech. Syst. Signal Process. (2021), https://doi.org/10.1016/j.ymssp.2020.107423.
[11] W. Ochoński, Sliding bearings lubricated with magnetic fluids, Ind. Lubr. Tribol. 59 (2007) 252–265, https://doi.org/10.1108/00368790710820856.
[12] H. Urreta, Z. Leicht, A. Sanchez, A. Agirre, P. Kuzhir, G. Magnac, Hydrodynamic bearing lubricated with magnetic fluids, J. Intell. Mater. Syst. Struct. 21 (2010) 1491–1499, https://doi.org/10.1177/1045389X09356007.
[13] N. Vaz, K.G. Binu, P. Serrao, M.P. Hemanth, J. Jacob, N. Roy, E. Dias, Experimental investigation of frictional force in a hydrodynamic journal bearing lubricated with magnetorheological fluid, J. Mech. Eng. Autom. 7 (2017) 131–134, https://doi.org/10.5923/j.jmea.20170705.01.
[14] A.C. Becnel, W. Hu, N.M. Wereley, Measurement of magnetorheological fluid properties at shear rates of up to 25 000 s-1, IEEE Trans. Magn. 48 (2012) 3525–3528, https://doi.org/10.1109/TMAG.2012.2207707.
[15] X. Wang, H. Li, G. Meng, Rotordynamic coefficients of a controllable magnetorheological fluid lubricated floating ring bearing, Tribol. Int. (2017), https://doi.org/10.1016/j.triboint.2017.04.002.
[16] W. Horak, J. Salwiński, M. Szczęch, Analysis of the Influence of Selected Factors on the Capacity of Thrust Sliding Bearings Lubricated with Magnetic Fluids, Tribologia, 2017, pp. 33–38, https://doi.org/10.5604/01.3001.0010.5988.
[17] S.G.E. Lampaert, R.A.J. van Ostayen, Experimental results on a hydrostatic bearing lubricated with a magnetorheological fluid, Curr. Appl. Phys. (2019), https://doi.org/10.1016/j.cap.2019.09.004.
[18] F. Quinci, W. Litwin, M. Wodtke, R. van den Nieuwendijk, A comparative performance assessment of a hydrodynamic journal bearing lubricated with oil and magnetorheological fluid, Tribol. Int. (2021), https://doi.org/10.1016/j.triboint.2021.107143.
[19] G.H.G. van der Meer, F. Quinci, W. Litwin, M. Wodtke, R.A.J. van Ostayen, Experimental comparison of the transition speed of a hydrodynamic journal bearing lubricated with oil and magnetorheological fluid, Tribol. Int. (2023), https://doi.org/10.1016/j.triboint.2023.108976.
[20] S. Li, S. Xiu, W. Song, C. Sun, H. Yang, Research on the wear characteristics of magnetorheological fluid in sealing interface considering the interaction between surface roughness and magnetic particles, Tribol. Int. (2023), https://doi.org/10.1016/j.triboint.2023.108496.
[21] M.M. Khonsari, E.R. Booser, Effect of contamination on the performance of hydrodynamic bearings, Proc. Inst. Mech. Eng. Part J J. Eng. Tribol. 220 (2006) 419–428, https://doi.org/10.1243/13506501J00705.
[22] G.K. Nikas, A state-of-the-art review on the effects of particulate contamination and related topics in machine-element contacts, Proc. Inst. Mech. Eng. Part J J. Eng. Tribol. (2010), https://doi.org/10.1243/13506501JET752.
[23] J.K. Duchowski, K.G. Collins, W.M. Dmochowski, Experimental evaluation of filtration requirements for journal bearings operating under different contaminant levels, Lubr. Eng. 58 (2002) 34–39.
[24] R.C. Elwell, Foreign object damage in journal bearings., lubr, Eng. 34 (1978) 187–192.
[25] V. Wikström, E. Höglund, R. Larsson, Wear of bearing liners at low speed rotation of shafts with contaminated oil, Wear 162–164 (1993) 996–1001, https://doi.org/10.1016/0043-1648(93)90110-8.
[26] J.L. Xuan, I.T. Hong, E.C. Fitch, Hardness effect on three-body abrasive wear under fluid film lubrication, J. Tribol. (1989), https://doi.org/10.1115/1.3261876.
[27] P.L. Wong, W.A. Bullough, C. Feng, S. Lingard, Tribological performance of a magneto-rheological suspension, Wear (2001), https://doi.org/10.1016/S0043-1648(00)00507-X.
[28] W.C. Leung, W.A. Bullough, P.L. Wong, C. Feng, The effect of particle concentration in a magneto rheological suspension on the performance of a boundary lubricated contact, Proc. Inst. Mech. Eng. Part J J. Eng. Tribol. (2004), https://doi.org/10.1243/1350650041762622.
[29] W.L. Song, S.B. Choi, J.Y. Choi, C.H. Lee, Wear and friction characteristics of magnetorheological fluid under magnetic field activation, Tribol. Trans. (2011), https://doi.org/10.1080/10402004.2011.584365.
[30] Z.D. Hu, H. Yan, H.Z. Qiu, P. Zhang, Q. Liu, Friction and Wear of Magnetorheological Fluid Under Magnetic Field, Wear, 2012, https://doi.org/10.1016/j.wear.2012.01.006.
[31] A.J.F. Bombard, J. De Vicente, Boundary lubrication of magnetorheological fluids in PTFE/steel point contacts, Wear (2012), https://doi.org/10.1016/j.wear.2012.08.012.
[32] K. Shahrivar, A.L. Ortiz, J. De Vicente, A comparative study of the tribological performance of ferrofluids and magnetorheological fluids within steel-steel point contacts, Tribol. Int. (2014), https://doi.org/10.1016/j.triboint.2014.05.008.
[33] Z. Hu, H. Zhang, H. Zhao, D. Wang, The friction and Wear behavior of Silicon oil-based Magnetorheological fluid with solid lubricant, J. Phys. Conf. Ser. (2022), https://doi.org/10.1088/1742-6596/2174/1/012029.
[34] S. Zhang, Z. Long, X. Yang, Lubrication performance of magnetorheological fluid-lubricated rubber stern bearing test ring, J. Brazilian Soc. Mech. Sci. Eng. (2021), https://doi.org/10.1007/s40430-020-02796-3.
[35] Liquids Research Ltd., Magneto-Rheological Fluids.Pdf, Web Page. (n.d.). https://liquidsresearch.com/en-GB/document_download-58.aspx (accessed November 27, 2024).
[36] COMSOL AB, COMSOL multiphysics® Version 6.2. https://www.comsol.com/, 2025. (Accessed 19 August 2025).
[37] C.A. Schneider, W.S. Rasband, K.W. Eliceiri, NIH Image to ImageJ: 25 years of image analysis, Nat. Methods (2012), https://doi.org/10.1038/nmeth.2089.
[38] C.H. Li, P.K.S. Tam, An iterative algorithm for minimum cross entropy thresholding, Pattern Recognit. Lett. (1998), https://doi.org/10.1016/S0167-8655(98)00057-9.
[39] G. Bossis, O. Volkova, S. Lacis, A. Meunier, Magnetorheology: fluids, structures and rheology. https://doi.org/10.1007/3-540-45646-5_11, 2002.
[40] C.L. Dong, C.Q. Yuan, X.Q. Bai, Y. Yang, X.P. Yan, Study on Wear Behaviours for NBR/stainless Steel Under Sand water-lubricated Conditions, Wear, 2015, https://doi.org/10.1016/j.wear.2015.01.009.
[41] M. xue Shen, B. Li, S. Li, G. yao Xiong, D. hui Ji, Z. nan Zhang, Effect of particle concentration on the tribological properties of NBR sealing pairs under contaminated water lubrication conditions, Wear 456–457 (2020) 203381, https://doi.org/10.1016/j.wear.2020.203381.
[42] G. Hu, J. Ma, G. Yuan, K. Shen, H. Wang, Effect of hard particles on the tribological properties of hydrogenated nitrile butadiene rubber under different lubricated conditions, Tribol. Int. (2022), https://doi.org/10.1016/j.triboint.2022.107457.
[43] R. Zuo, G. Wang, G. Hu, S. Zhao, G. Wei, Tribological properties of hydrogenated nitrile rubber in confrontation with hard particles under different axial loads, Tribol. Int. 153 (2021) 106649, https://doi.org/10.1016/j.triboint.2020.106649.
[44] G. van der Meer, R. van Ostayen, Investigating film thickness and friction of an MR-Lubricated journal bearing, Lubricants 13 (2025), https://doi.org/10.3390/lubricants13040171.